The human iliotibial band is specialized for elastic energy storage compared with the chimp fascia lata

© 2015. Published by The Company of Biologists Ltd | The Journal of Experimental Biology (2015) 218, 2382-2393 doi:10.1242/jeb.117952

RESEARCH ARTICLE

The human iliotibial band is specialized for elastic energy storage compared with the chimp fascia lata

Carolyn M. Eng[1,2,*], Allison S. Arnold[1], Andrew A. Biewener[1] and Daniel E. Lieberman[2]

ABSTRACT

This study examines whether the human iliotibial band (ITB) is specialized for elastic energy storage relative to the chimpanzee fascia lata (FL). To quantify the energy storage potential of these structures, we created computer models of human and chimpanzee lower limbs based on detailed anatomical dissections. We characterized the geometry and force–length properties of the FL, tensor fascia lata (TFL) and gluteus maximus (GMax) in four chimpanzee cadavers based on measurements of muscle architecture and moment arms about the hip and knee. We used the chimp model to estimate the forces and corresponding strains in the chimp FL during bipedal walking, and compared these data with analogous estimates from a model of the human ITB, accounting for differences in body mass and lower extremity posture. We estimate that the human ITB stores 15- to 20-times more elastic energy per unit body mass and stride than the chimp FL during bipedal walking. Because chimps walk with persistent hip flexion, the TFL and portions of GMax that insert on the FL undergo smaller excursions (origin to insertion) than muscles that insert on the human ITB. Also, because a smaller fraction of GMax inserts on the chimp FL than on the human ITB, and thus its mass-normalized physiological cross-sectional area is about three times less in chimps, the chimp FL probably transmits smaller muscle forces. These data provide new evidence that the human ITB is anatomically derived compared with the chimp FL and potentially contributes to locomotor economy during bipedal locomotion.

KEY WORDS: Elastic energy storage, Iliotibial band, Fascia, Musculoskeletal modeling, Chimpanzee anatomy

INTRODUCTION

Bipedalism appears to be the initial derived feature that set the human lineage on a separate evolutionary trajectory from the African great apes (Darwin, 1871; Haile-Selassie, 2001; Zollikofer et al., 2005). There are many hypotheses about the selective pressures that favored the origin of hominin bipedalism, but one of the most widely accepted is that natural selection favored bipedal walking over more costly quadrupedal gaits, such as knuckle-walking, to reduce the energetic costs of travel as climatic shifts increased the distances between food sources (Rodman and McHenry, 1980; Sockol et al., 2007). This idea is supported by evidence that many adaptations in the lower limb associated with bipedalism, such as relatively longer limbs and shorter toes, also benefit locomotor economy (Pontzer, 2007; Rolian et al., 2009).

[1]Department of Organismic and Evolutionary Biology, Harvard University, Cambridge, MA 02138, USA. [2]Department of Human Evolutionary Biology, Harvard University, Cambridge, MA 02138, USA.

*Author for correspondence (carolyn_eng@brown.edu)

Received 8 December 2014; Accepted 18 May 2015

The iliotibial band (ITB) is a unique structure in the human lower limb, derived from the fascia lata (FL) of the thigh, which may contribute to locomotor economy (Fig. 1). The ITB is not present in other apes and thus almost certainly evolved independently in hominins, but its role in human locomotion is not well understood. Although the most common view of the ITB's function is to stabilize the pelvis in the frontal plane (Inman, 1947; Kaplan, 1958; Stern, 1972; Gottschalk et al., 1989), we recently created a musculoskeletal model of the ITB to investigate whether forces generated by the tensor fascia lata (TFL) or gluteus maximus (GMax) substantially stretch the ITB during running, storing elastic energy that is recovered later in the stride (Eng et al., 2015). We estimated that the anterior ITB stores about 1 J of energy per stride during the late stance and early swing phases, whereas the posterior ITB stores about 6 J per stride during the late swing phase at fast running speeds (5 m s^{-1}). Here, we interpret these findings within a broader comparative context by examining whether the chimp FL also stores elastic energy or whether the capacity of the human ITB to store energy during locomotion is unique to humans among apes. This study also examines whether the human ITB has a greater capacity than the chimp FL to transmit moments that stabilize the pelvis in the frontal plane during walking.

Chimpanzees (Hominidae: *Pan*) are a key comparative species for interpreting the derived nature of the ITB because chimps are the extant sister taxon to *Homo* (Ruvolo, 1994; Satta et al., 2000). Given the many morphological similarities between chimps and gorillas, with many differences likely resulting from the effects of size (Shea, 1985; Berge and Penin, 2004), it is most parsimonious to infer that the last common ancestor (LCA) of *Pan* and humans resembled *Pan* in morphology and was a knuckle-walking ape with no ITB (Pilbeam, 1996; Wrangham and Pilbeam, 2001; but see Sayers and Lovejoy, 2008; Lovejoy, 2009; Almécija et al., 2013). It is also possible that the ITB was convergently lost in both gorillas and chimpanzees, but given the lack of an ITB in other apes (Swindler and Wood, 1973; Sigmon, 1975), it is reasonable to assume that the ITB is a human autapomorphy. Therefore, this study compares the function of the human ITB with that of the chimp FL using musculoskeletal models developed from detailed anatomical experiments.

The ability of fascial connective tissues to store elastic energy depends in part on the muscular forces these tissues transmit, which likely differ between chimps and humans. Estimating these forces during walking requires information about the activation patterns, force–length properties and excursions of the inserting muscles. However, descriptions of relevant chimp anatomy in the literature vary considerably and are limited by small sample sizes (Stern, 1972; Swindler and Wood, 1973; Sigmon, 1975; Sigmon and Farslow, 1986). According to most studies, the TFL inserts on the chimp FL (Sigmon, 1974, 1975; Sigmon and Farslow, 1986), as it does on the human ITB. However, compared with the human TFL, the chimp TFL is thought to be smaller and partially fused with the anteriormost portion of the cranial GMax (Sigmon, 1974, 1975;

The Journal of Experimental Biology

The Journal of Experimental Biology (2015) 218, 2382-2393 doi:10.1242/jeb.117952

List of symbols and abbreviations

a	effective cross-sectional area
E	elastic modulus
E_{FL}	elastic energy storage in the fascia lata
F_{FL}	force transmitted by the fascia lata
FL	fascia lata
FL_{ant}	anterior fascia lata
FL_{post}	posterior fascia lata
F_{max}	maximum muscle isometric force
GMax	gluteus maximus
GMaxCd	caudal head of gluteus maximus
GMaxCr	cranial head of gluteus maximus
ITB	iliotibial band
$\tilde{k}$	normalized stiffness
L_f	fiber length
L_M	muscle length
L_{opt}	optimal fiber length
L_{TS}	tendon slack length
M	mass
MTU	muscle–tendon unit
PCSA	physiological cross-sectional area
TFL	tensor fascia lata
ΔL_{FL}	length change of the fascia lata
ρ	muscle density

Sigmon and Farslow, 1986). When referring to the GMax in chimps, we distinguish between the cranial portion (GMaxCr; also called gluteus maximus proprius) and the caudal portion (GMaxCd; also called ischiofemoralis). There is general agreement that GMaxCr is thinner and less massive than the homologous GMax in humans (Stern, 1972; Swindler and Wood, 1973; Sigmon, 1975; Lieberman et al., 2006), but there is a lack of consensus about where GMaxCr inserts. Some studies report that GMaxCr inserts on the FL (Swindler and Wood, 1973; Sigmon, 1974, 1975), but others report that insertion on the FL is rare (Preuschoft, 1961; Stern, 1972). The GMaxCd is thought to insert not into the chimp FL, but along the femoral shaft from the gluteal tuberosity to the lateral epicondyle; this muscle is absent in humans (Stern, 1972; Sigmon, 1974, 1975). Thus, characterizing the energy storage capacity of the chimp FL required us to identify more definitively the portions of TFL, GMaxCr and GMaxCd that insert on the chimp FL and to characterize the muscle architecture of these muscles.

The amount of elastic energy stored by the chimp FL and the human ITB during walking also depends on the length changes of these fascial tissues, which depend on the length changes of the muscle–tendon units (MTUs). These length changes depend on the moment arms of the MTUs about the hip and knee and the changes in hip and knee angles during walking. Because moment arms generally vary as a function of joint angle (An et al., 1984; Hoy et al., 1990; Spoor et al., 1990), published descriptions of chimp moment arms based solely on bone morphology may not accurately predict changes in MTU length during walking. Thus, characterizing the energy storage capacity of the chimp FL also required us to measure the moment arms of TFL, GMaxCr and GMaxCd in chimpanzee cadavers over the ranges of hip and knee angles corresponding to walking. Although moment arm data are available for several chimp muscles (Thorpe et al., 1999; Payne et al., 2006; Holowka and O'Neill, 2013), and a detailed model of the chimp lower limb has been developed based on these data (O'Neill et al., 2013), the moment arms of TFL and the portions of GMax that insert on the FL have not previously been reported.

It is commonly thought that the human ITB functions to stabilize the pelvis in the frontal plane when tensed by the inserting muscles

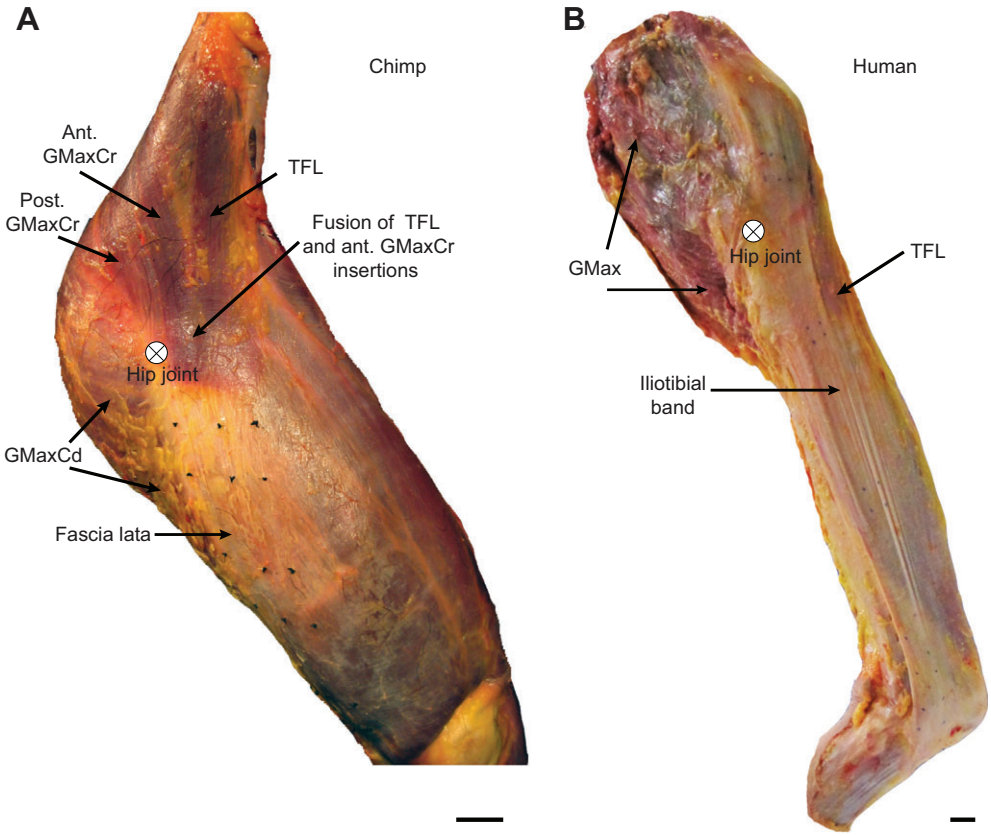

Fig. 1. Lateral view of the chimpanzee and human lower limbs. (A) The chimp limb shows the distal fusion of the TFL and anterior GMaxCr muscle fibers proximal to where they insert in the anterior FL. The posterior GMaxCr fibers insert in the lateral femur. The superficial GMaxCd fibers insert in the posterior FL. The locations of suture marker pairs (visible as black dots) in the anterior and posterior FL were tracked with high-speed video and used to determine the hip and knee angles at which the anterior and posterior FL began to stretch. (B) In the human limb, TFL inserts in the anterior ITB, while a portion of GMax fibers inserts in the posterior ITB. Although the human GMax is homologous to the chimp GMaxCr, $GMax–ITB_{post}$ energy storage was compared with $GMaxCd–FL_{post}$ energy storage because of the posterior insertions of the muscles and similar hip extension moment arms. Scale bars: 2 cm.

The Journal of Experimental Biology (2015) 218, 2382-2393 doi:10.1242/jeb.117952

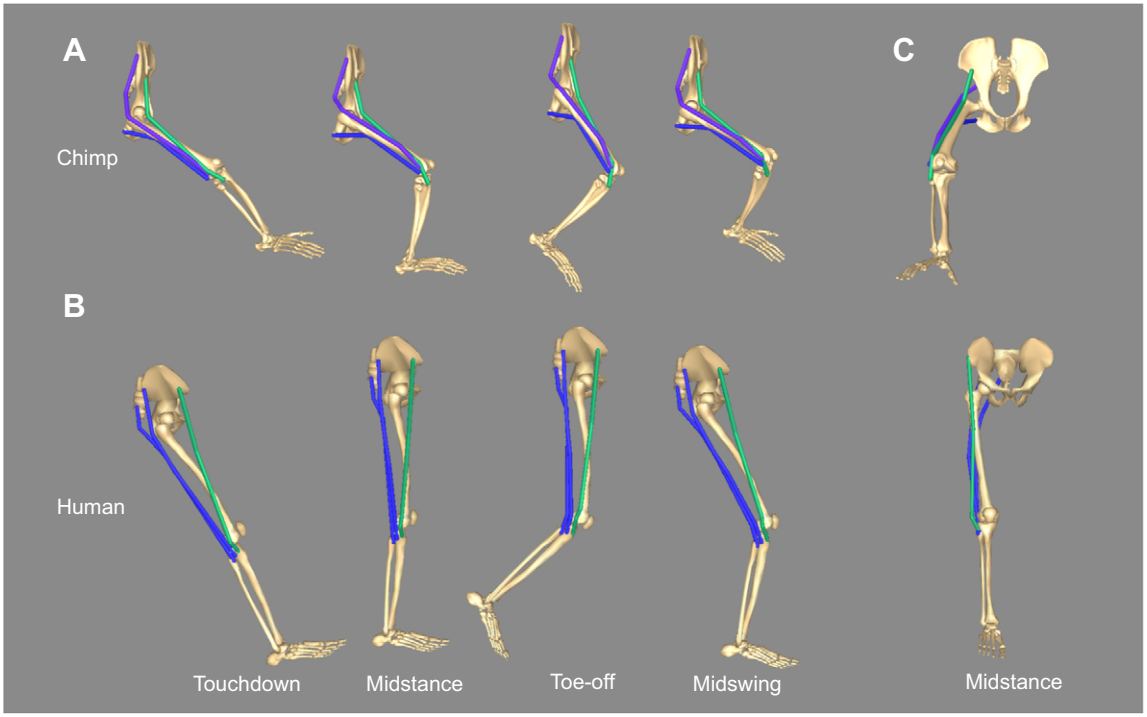

Fig. 2. Chimpanzee and human lower extremity models during bipedal walking. (A) Lateral view of the chimp model modified from O'Neill et al. (2013) showing FL MTUs including TFL–FL_{ant} (green), GMaxCr–FL_{ant} (purple) and GMaxCd–FL_{post} (blue) during touchdown, midstance, toe-off and midswing during bipedal walking. (B) Lateral view of the human model from Eng et al. (2015) showing ITB MTUs including TFL–ITB_{ant} (green) and GMax–ITB_{post} (blue) during bipedal walking. The human GMax–ITB_{post} MTU is color-coded based on its insertion in the posterior ITB and not based on homology. (C) Anterior view of the chimp (top) and human (bottom) models during midstance, showing the abducted position of the chimp hip during bipedal walking.

(Inman, 1947; Kaplan, 1958; Stern, 1972; Gottschalk et al., 1989). Unlike quadrupedal apes, bipedal hominins must stabilize the body's center of mass over a small area of support. Thus, selection for increased abduction moment capacity may have acted on the ITB or other structures to help stabilize the pelvis in the frontal plane during walking. In this study, we used our musculoskeletal models to compare the frontal plane moments transmitted by the chimp FL and the human ITB during midstance.

In summary, we measured the masses, fascicle lengths, pennation angles, and moment arms of the TFL and GMax in four chimpanzee cadavers. These data were used to refine a 3D musculoskeletal model of the chimp hindlimb (O'Neill et al., 2013) that includes the attachments and force–length properties of the FL and the inserting muscles. The model was used with kinematic descriptions of the chimp's hip and knee angles during bipedal walking to compute the forces and corresponding strains in the chimp FL and to predict its capacity for elastic energy storage and recovery (Fig. 2). Results were compared with analogous data from a model of the human ITB (Eng et al., 2015) to test four specific hypotheses: (H1) the muscles inserting on the human ITB have a greater force-generating capacity

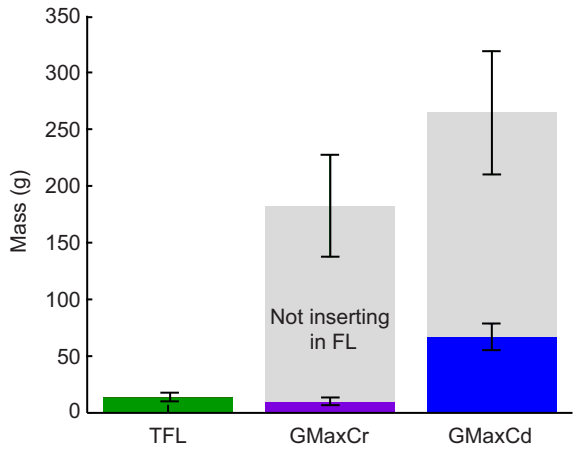

Fig. 3. Mass of the chimpanzee TFL, GMaxCr and GMaxCd muscles inserting on the FL versus the femur. All of the TFL muscle mass inserts in the chimp FL, but only 5% of the GMaxCr mass and 25% of the GMaxCd mass inserts in the FL.

Table 1. Muscle architecture of the chimpanzee tensor fascia lata, cranial gluteus maximus and caudal gluteus maximus muscles

Muscle	Mass (g)	Fascicle length (cm)	Pennation angle (deg)	PCSA (cm^2)*
TFL	14.0±3.8	121.8±1.5	1.7±1.7	1.2±0.4
GMaxCr1‡	10.2±3.4	107.2±6.0	5.0±2.9	0.7±0.6
GMaxCr2	84.3±21.0	85.2±8.9	22.3±6.7	10.0±3.3
GMaxCr3	88.1±25.5	85.3±12.4	22.3±6.7	9.7±4.9
GMaxCd1§	94.2±22.4	123.0±3.8	18.3±3.3	7.8±2.0
GMaxCd2	103.3±32.1	170.0±20.0	18.3±1.7	6.5±1.7
GMaxCd3	29.4±7.8	178.7±11.3	16.7±3.3	2.0±0.2
GMaxCd4	37.5±4.2	149.0±19.7	16.7±1.7	2.7±0.3

Data are expressed as means±s.e.m. Shaded muscle regions do not insert on the FL.

*Pennation angle is not included in the PCSA calculation because our SIMM model multiplies PCSA, specific tension and pennation angle to determine the maximum isometric force of a muscle.

‡GMaxCr1 represents the anteriormost muscle portion, whereas GMaxCr3 the posteriormost muscle portion.

§GMaxCd1 represents the superiormost muscle portion, whereas GMaxCd4 the inferiormost muscle portion.

The Journal of Experimental Biology (2015) 218, 2382-2393 doi:10.1242/jeb.117952

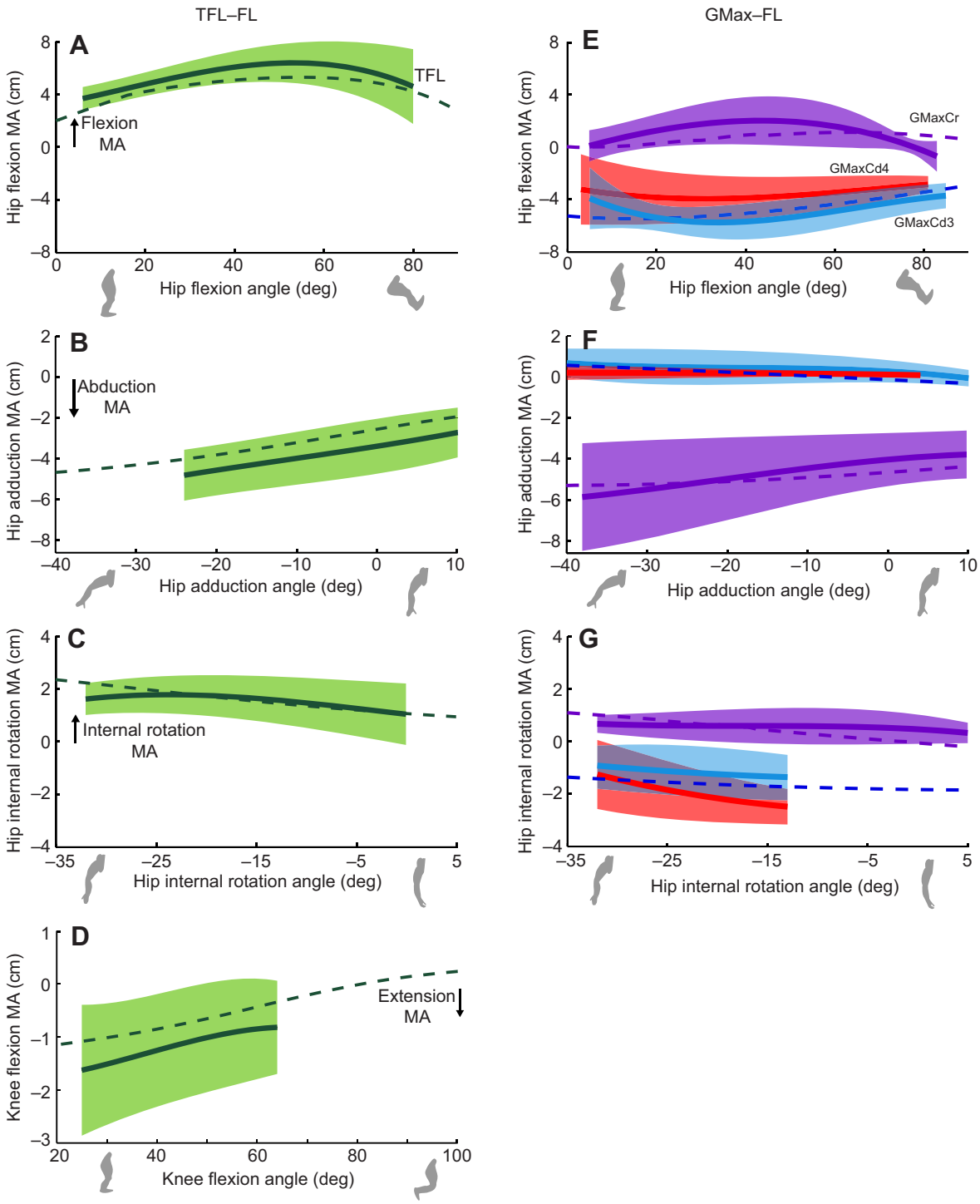

Fig. 4. Hip and knee moment arms of TFL and GMax MTUs compared with experimental data. (A) TFL has a large hip flexion moment arm (MA). (B) TFL has a large hip abduction moment arm that increases as the hip abducts (negative values of hip adduction). (C) TFL has an internal rotation moment arm that increases with external rotation. (D) TFL has a small knee extension moment arm that increases with knee extension. (E) All portions of GMaxCd–FL_{post} have large hip extension moment arms that increase with hip extension; GMaxCr–FL_{ant} has a small hip flexion moment arm. (F) All portions of GMaxCd–FL_{post} have small hip adduction moment arms, whereas GMaxCr–FL_{ant} has a large hip abduction moment arm that increases with hip abduction. (G) All portions of GMaxCd–FL_{post} have external rotation moment arms; GMaxCr–FL_{ant} has an external rotation moment arm. Solid lines and shaded regions indicate the means and s.d. of experimentally determined moment arms from four cadaveric limbs. Dashed lines show the moment arms of TFL–FL_{ant} (green), GMaxCr–FL_{ant} (purple), and the combined path of GMaxCd3,4–FL_{post} (blue) predicted by our chimp model.

than the muscles inserting on the chimp FL, accounting for differences in body mass; (H2) the human ITB undergoes greater strains than the chimp FL during typical bipedal kinematics; (H3) the human ITB has a substantially greater potential to store elastic energy per unit body mass than the chimp FL during bipedal walking; (H4) the human ITB transmits substantially larger

The Journal of Experimental Biology (2015) 218, 2382-2393 doi:10.1242/jeb.117952

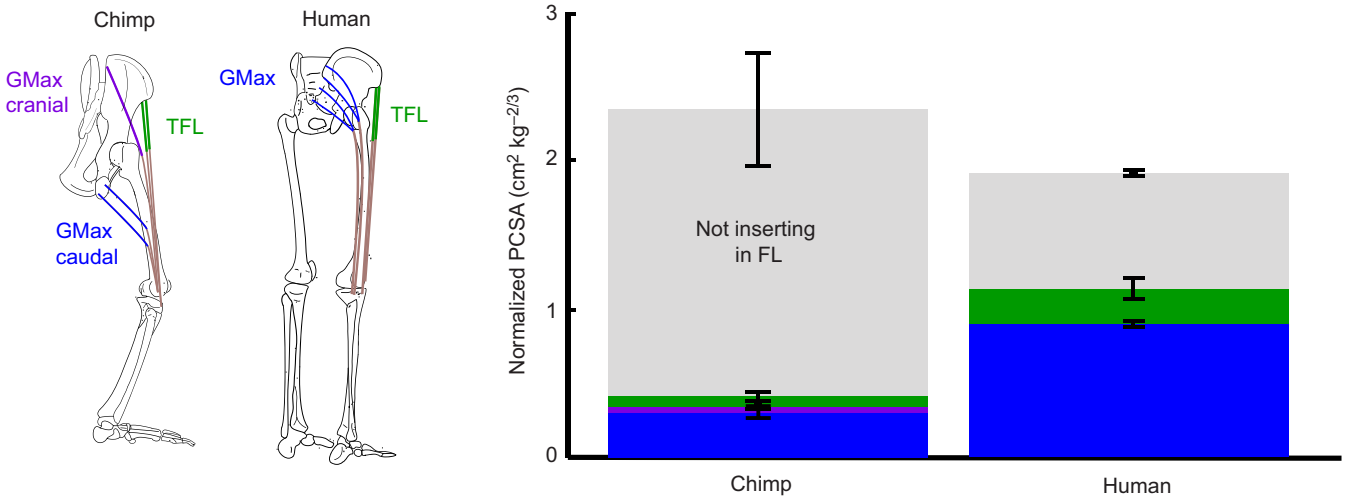

Fig. 5. The muscles inserting on the human ITB have the potential to transmit substantially larger forces than muscles inserting on the chimp FL. Normalized muscle PCSA (PCSA/body mass$^{2/3}$) for the portions of TFL (green), GMaxCr (purple) and GMaxCd (blue) that insert in the chimp FL or human ITB compared with the total normalized PCSA of the muscle regions not inserting in the FL or ITB.

moments about the hip in the frontal plane than the chimp FL during midstance, which would provide some evidence that the human ITB may be specialized for frontal plane stability.

RESULTS

Description of muscle attachments, mass and moment arms in chimps

Dissections of the chimp TFL, GMaxCr and GMaxCd revealed that portions of all three muscles insert directly on the FL (Fig. 3). All TFL muscle fibers insert into the anterior FL (TFL–FL_{ant}). Consistent with findings from some previous studies (Sigmon, 1974, 1975; Sigmon and Farslow, 1986), our dissections confirmed that the anterior portion of the chimp GMaxCr is fused distally with the TFL and inserts into the anterior FL (Fig. 1A). However, this portion of GMaxCr (GMaxCr–FL_{ant}) is relatively small, constituting only about 5% of the muscle's total mass (Table 1). Our dissections also revealed that about 25% of the chimp GMaxCd mass (GMaxCd–FL_{post}) inserts into the posterior FL, consistent with most other reports of chimpanzee anatomy (Champneys, 1871; Sigmon and Farslow, 1986) except Stern (1972).

Moment arm measurements revealed that muscles inserting in the anterior FL flex and abduct the hip, whereas muscles inserting in the posterior FL extend and adduct the hip (Fig. 4). In particular, the chimp TFL–FL_{ant} has a relatively large hip flexion moment arm. The GMaxCr–FL_{ant} has a large hip abduction moment arm, but a very small hip flexion moment arm. The chimp GMaxCd–FL_{post} has a small hip adduction moment arm, but a relatively large hip extension moment arm that increases with hip extension. The moment arms predicted by our model are consistent with results from our tendon excursion measurements (Fig. 4).

Biomechanically, we found that the chimp GMaxCd–Fl_{post} is more comparable to the portion of the human GMax that inserts on the ITB (GMax–ITB_{post}) than is the homologous chimp GMaxCr–$FL_{ant.}$ The chimp GMaxCr–FL_{ant} has a smaller mass and a more anterior insertion than the human GMax–ITB_{post}. By contrast, large portions of both the chimp GMaxCd and the human GMax insert posteriorly on the FL and ITB, respectively, and these muscles have similar hip extension moment arms. Therefore, to test our hypotheses, we compared the force-generating capacity and energy storage potential of the human GMax–ITB_{post} with predictions generated by our model of the chimp GMaxCd–FL_{post}.

Comparison of muscle force-generating capacity

Muscles inserting on the human ITB have the potential to transmit substantially larger forces to the ITB than the muscles inserting on the chimp FL transmit to the FL (Fig. 5). The force-generating capacity of the human TFL is significantly larger than that of the chimp TFL, even after accounting for differences in body mass. In particular, the normalized physiological cross-sectional area (PCSA) of the human TFL (0.24±0.07 $cm^2\ kg^{-2/3}$) is more than three times greater than that of the chimp TFL (0.07±0.03 $cm^2\ kg^{-2/3}$; $P<0.05$). The normalized PCSA of the human GMax–ITB_{post} is more than double that of the chimp GMaxCd–FL_{post} (0.72±0.13 $cm^2\ kg^{-2/3}$ versus 0.30±0.04 $cm^2\ kg^{-2/3}$; $P<0.05$). These data suggest that the human ITB transmits substantially larger muscle forces than the chimp FL.

Comparison of elastic energy storage capacity during bipedal walking

The ITB MTUs in the human model undergo substantially greater length changes than the FL MTUs in the chimp model during bipedal walking (Fig. 6). These larger MTU excursions are not simply a result of larger human limbs. Rather, these data reflect differences between the moment arms of the chimp FL MTUs (Fig. 4) and the moment arms of the human ITB MTUs (Eng et al., 2015), as well as measured differences in hip and knee angles during walking.

In humans, the TFL stretches when it is active in late stance, similar to the TFL in chimps (Fig. 7). The GMax also stretches when it is active; this lengthening occurs during late swing in the human GMax–ITB_{post} and during early stance in the chimp GMaxCd–FL_{post} (Fig. 7). However, because humans extend their hips more than chimps during bipedal walking (~45 deg range in humans, from −20 deg extension to 25 deg flexion, versus ~25 deg range in chimps, from 25 to 50 deg flexion; O'Neill et al., 2015), human ITB MTUs undergo substantially greater length changes than chimp FL MTUs throughout the gait cycle (Fig. 6). The human TFL–ITB_{ant} stretches more than the chimp TFL–FL_{ant} in late stance because of a larger hip flexion moment arm (slope of the line in Fig. 6B versus A) and the greater hip flexion/extension excursion in humans. The human GMax–ITB_{post} also stretches more than the chimp GMaxCd–FL_{post} because of the greater hip flexion excursion in humans.

Because human ITB MTUs undergo relatively larger length changes during bipedal walking, and because the force-generating

The Journal of Experimental Biology (2015) 218, 2382-2393 doi:10.1242/jeb.117952

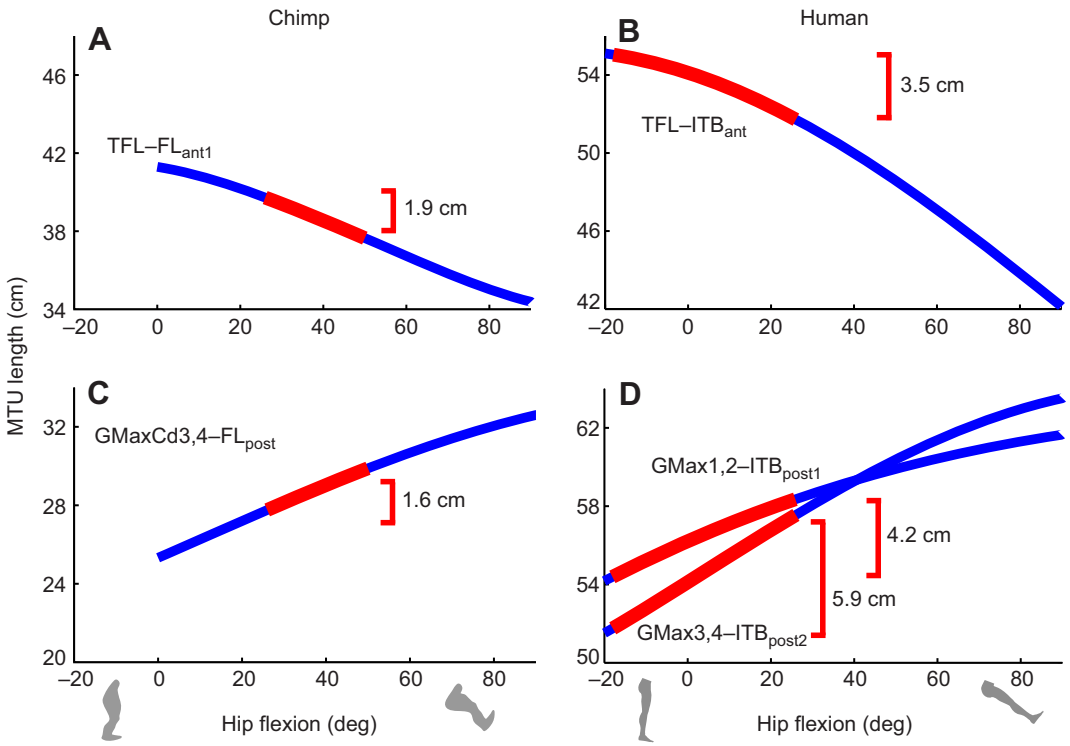

Fig. 6. MTU length as a function of hip flexion in the chimp FL and human ITB. MTU length in the anterior chimp FL (A), anterior human ITB (B) and the posterior chimp FL (C) and posterior human ITB (D). The thickened red regions show the range of hip flexion/extension angles during bipedal walking, which is lower in chimps compared with humans. The brackets indicate the change in MTU length occurring during bipedal walking due to changes in hip flexion/extension. The slope of the curve is equivalent to the moment arm of the MTU.

capacity of human muscles inserting on the ITB is larger relative to the force-generating capacity of chimp muscles inserting on the FL, the human ITB has a greater potential to store energy than the chimp FL (Fig. 8). Activating GMax at 20% during late swing in the human model generates force that stretches the posterior ITB by about 4% and stores 0.0133 J kg^{-1} of elastic energy per stride (Fig. 8A,C). Activating GMaxCd at 20% during midstance in the chimp model strains the posterior FL by a similar amount, but stores only 0.0009 J kg^{-1} of elastic energy per stride. Activating TFL at 20% during late stance in the human model stretches the anterior ITB by 2% and stores 0.0018 J kg^{-1} of elastic energy per stride (Fig. 8B,D). Activating TFL at 20% during late stance in the chimp model stretches the anterior TFL less, storing only 0.0001 J kg^{-1} of elastic energy per stride. Energy storage increases with muscle activation level (Fig. 8). For example, activating the human GMax and chimp GMaxCd at 60% stores 0.0616 J kg^{-1} of elastic energy per stride in the human ITB and 0.0038 J kg^{-1} in the chimp FL (Fig. 8C), which is over four times the energy stored with 20% activation. With 60% activation of the TFL, the human ITB stores 0.0089 J kg^{-1} and the chimp FL stores 0.0006 J kg^{-1} (Fig. 8D).

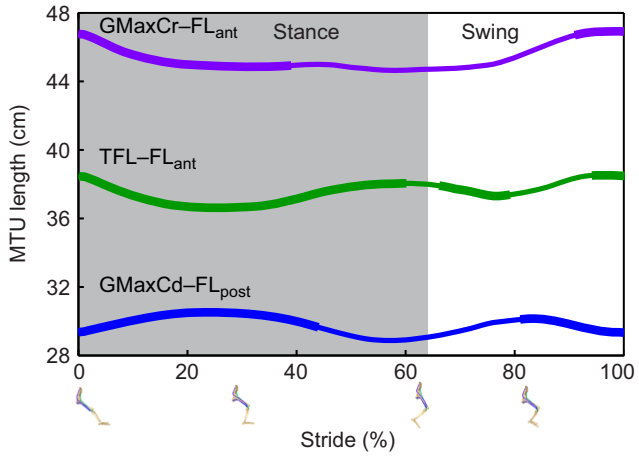

Fig. 7. MTU length during a stride of bipedal walking in the chimp. MTU length in TFL–FL$_{ant}$, GMaxCr–FL$_{ant}$ and GMaxCd–FL$_{post}$. Thickened portions of each curve denote periods in the stride when the muscles are active as recorded in Stern and Susman (1981). EMG recordings from chimps confirm that TFL, GMaxCr and GMaxCd are active when the MTU is stretched or at its maximum length.

Comparison of frontal plane moment-generating capacity during the stance phase

When we maximally activated muscles inserting in the ITB and FL at midstance in our models, we found that the frontal plane moment transmitted via the human ITB is not substantially greater than the moment transmitted via the chimp FL (Fig. 9) after normalizing the moments by body weight and hemi-pelvis width. In both models, the TFL and anterior GMax MTUs have the capacity to generate small moments about the hip that help support the pelvis. By contrast, the MTUs with the greatest force-generating capacity, GMax3,4–ITB$_{post}$ in the human and GMaxCd–FL$_{post}$ in the chimp, both generate an opposing moment at the hip that pulls the pelvis inferiorly. If we ignore GMax3,4–ITB$_{post}$ in the human model, we estimate that the ITB transmits about 10% of the total frontal plane moment-generating capacity of all muscles inserting on the ITB and femur (Fig. 9), which is greater than our estimate of the percentage transmitted by the chimp FL (3%). However, if GMax3,4 is activated with other portions of GMax during walking, the summed contribution of the human ITB MTUs to the frontal plane moment is negligible. In summary, this

The Journal of Experimental Biology (2015) 218, 2382-2393 doi:10.1242/jeb.117952

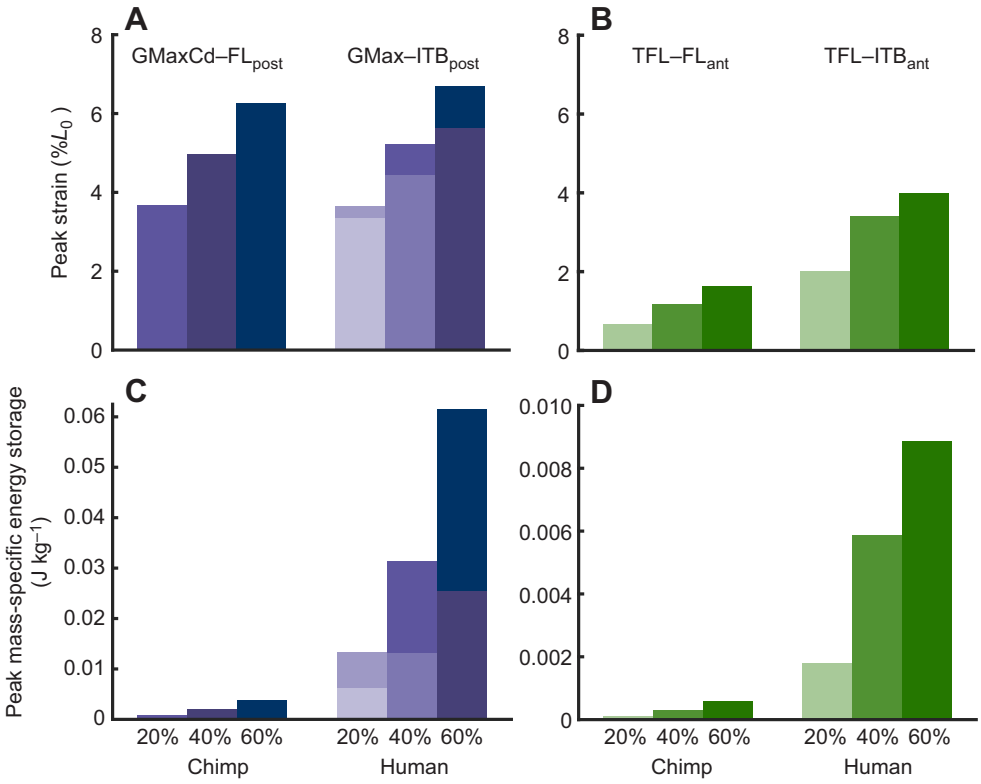

Fig. 8. Peak energy storage is greater in the human ITB than in the chimp FL. (A) Peak posterior chimp FL and human ITB strain during bipedal walking when the muscles are activated at 20, 40 and 60% of maximum. (B) Peak anterior chimp FL and human ITB strain when the muscles are activated at 20, 40 and 60% of maximum. (C) Peak elastic energy storage in the posterior chimp FL and human ITB during bipedal walking when the muscles are activated at 20, 40 and 60% of maximum. (D) Peak elastic energy storage in the anterior chimp FL and human ITB during bipedal walking when the muscles are activated at 20, 40 and 60% of maximum. For the posterior human ITB, the GMax1,2–ITB$_{post}$ is shown in light purple, whereas the GMax3,4–ITB$_{post}$ is shown in dark purple.

analysis provides little evidence that the human ITB is specialized to transmit forces in the frontal plane to stabilize the pelvis and support the torso against gravity during walking.

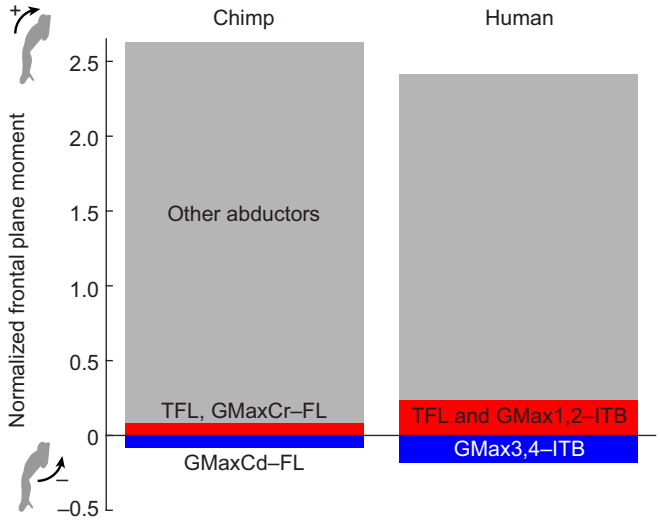

Fig. 9. The maximum frontal plane moment transmitted to the chimp FL and human ITB relative to the maximum frontal plane moment transmitted by the other hip abductors to the femur. Frontal plane moments (transmitted when muscle activation is 100%) are normalized by body mass and hemi-pelvis width. In both the human and chimp, the TFL and anterior GMax MTUs (red) have the capacity to generate small frontal plane moments about the hip that help support the pelvis and torso. By contrast, GMax3,4–ITB$_{post}$ in the human (blue) and GMaxCd–FL$_{post}$ in the chimp (blue), both generate an opposing moment at the hip that pulls the pelvis inferiorly. Other hip abductors included in the chimp and human models are gluteus medius, gluteus minimus, piriformis, sartorius, rectus femoris; the chimp model also includes iliacus and the human model includes gemelli. The portions of the human GMax1,2 and chimp GMaxCr inserting in the femur were also included in this group.

DISCUSSION

This study tested whether the human ITB is specialized for elastic energy storage relative to the chimp FL. We conducted detailed anatomical experiments on the largest sample of chimp lower extremities to date, and we analyzed musculoskeletal models of both humans and chimps to test four hypotheses.

First, we asked whether the muscles inserting on the human ITB have a greater force-generating capacity than the muscles inserting on the chimp FL, after accounting for body mass (H1). We found that, in total, the force-generating capacity of the muscles inserting on the ITB is three times greater than the force-generating capacity of the muscles inserting on the FL, suggesting substantially greater forces are transmitted via the ITB compared with the FL. This greater capacity for force primarily stems from the fact that only about 10% of the chimp TFL, GMaxCr and GMaxCd mass inserts in the FL, whereas nearly 60% of the human TFL and GMax mass inserts in the ITB.

Second, we hypothesized that the human ITB undergoes greater strains than the chimp FL during typical bipedal walking kinematics (H2). We found that the greater MTU length changes and greater mass-specific force-generating capacity of the human TFL result in greater peak strains in the human anterior ITB than the chimp anterior FL. The anterior ITB in humans stretches more than the anterior FL in chimps because humans walk with greater hip flexion/extension excursion than chimps (O'Neill et al., 2015). Contrary to our hypothesis, peak strains in the posterior ITB and posterior FL are similar in our models. However, consistent with our third hypothesis that the human ITB has a substantially greater potential to store elastic energy, per unit body mass, than the chimp FL during bipedal walking (H3), the larger forces transmitted to the posterior ITB result in substantially greater energy storage. Thus, differences in both anatomy and locomotor mechanics between chimpanzees and humans determine the human ITB's greater elastic energy storage capacity compared with the chimp FL.

The Journal of Experimental Biology (2015) 218, 2382-2393 doi:10.1242/jeb.117952

We also tested the prevailing hypothesis that the ITB functions to stabilize the pelvis in the frontal plane (Inman, 1947; Kaplan, 1958; Stern, 1972; Gottschalk et al., 1989) by estimating the maximum frontal plane moments that could be transmitted via the human ITB and chimp FL at midstance. These analyses indicate, contrary to our hypothesis (H4), that the human ITB does not have a substantially greater capacity to transmit frontal plane moments about the hip than the chimp FL. The human ITB transmits only about 10% of the total hip frontal plane moment at midstance and its contribution to the total frontal plane moment is negligible when GMax3,4–ITB_{post} is included. Thus, these results do not suggest that the ITB is primarily specialized for frontal plane stability of the pelvis. Although the human ITB does provide a frontal plane moment, our results indicate that the human ITB was likely selected to store elastic strain energy for improved locomotor economy.

It is important to acknowledge the limitations of this analysis. First, in our chimp model, we scaled the muscle PCSAs by the same specific tension of 31.5 N cm^{-2} used in O'Neill et al. (2013), which is higher than the typically reported range of 17–25 N cm^{-2} (Bodine et al., 1987; Lucas et al., 1987; Greaser et al., 1988). Scaling the chimpanzee muscle PCSAs by a lower specific tension value would decrease our estimates of FL energy storage and further amplify the difference in energy storage between the chimp FL and human ITB. Because the human model's muscle parameters were based on data from elderly cadaveric specimens whose atrophied muscles likely underestimate muscle PCSAs for healthy human subjects, muscle PCSAs were scaled by a specific tension of 61 N cm^{-2} (Arnold et al., 2010). In the model of Arnold and colleagues, this value of specific tension predicts hip, knee and ankle joint moments that are consistent with the moments measured in healthy human subjects. If we use the higher specific tension value for both the human and chimp models, chimp FL energy storage values are doubled, but human ITB energy storage is still substantially greater.

Second, because we lack data describing chimp FL material properties, we assumed its elastic modulus was similar to the human ITB, taking into account the lower FL cross-sectional area when calculating normalized FL stiffness. If the chimp FL has a lower elastic modulus than the human ITB, we may have underestimated the capacity of the chimp FL for energy storage during walking. However, even if we make the chimp FL twice as compliant, peak mass-specific energy storage at 20% muscle activation is still nearly an order of magnitude lower in the chimp FL than in the human ITB.

Third, chimps may require greater hip extensor muscle activation to maintain their typical bent hip and bent knee posture, so the chimp GMaxCd may have greater activation than the human GMax during walking. Higher activations and muscle forces in the chimp GMaxCd would reduce differences in human ITB and chimp FL energy storage. However, even when GMaxCd is activated at 60% in our model, the chimp FL_{post} stores 70% less mass-specific elastic energy than the human ITB_{post} with 20% GMax activation.

Fourth, we estimated the force generated by each muscle at joint angles corresponding to bipedal walking and ignored the muscle force–velocity properties. If these muscles do not operate isometrically during walking, then we may have overestimated force and energy storage. However, muscles acting in series with long elastic tissues often operate isometrically over much of force development (e.g. Biewener and Roberts, 2000). Consistent with this, ultrasound-based studies of human gastrocnemius function show limited shortening until push-off (Lichtwark et al., 2007; Farris and Sawicki, 2012), and Arnold et al.'s simulations of human walking and running (2013) showed that the GMax muscle fiber velocities were low during walking. In Arnold et al.'s model, GMax inserts on the femur via a relatively stiff tendon, and this assumption likely amplifies the muscle's estimated shortening velocity. It is plausible that GMax would change length even less in the model if it were more accurately represented as inserting via the ITB.

A final limitation of our analyses is that primates other than chimpanzees may be under greater selective pressure to increase locomotor economy through energy storage and recovery. While the last common ancestor of humans and other apes was probably a knuckle-walker that resembled chimpanzees in some respects, compromises between adaptations for walking and for climbing probably explain why the chimpanzee's cost of locomotion is unusually high among mammals (Taylor and Rowntree, 1973; Taylor et al., 1982; Sockol et al., 2007; Pontzer et al., 2014). To better understand whether evolved changes in FL anatomy are indeed related to minimizing the cost of terrestrial locomotion, studies that examine FL function in additional primates are vital.

Our results show that the human ITB is specialized for elastic energy storage compared with the chimp FL, suggesting that modifications to the FL and surrounding muscles in hominins were selected to increase the economy of bipedal locomotion. The chimpanzee FL is likely to be a good model for the ancestral condition from which the derived human ITB evolved. Although the chimp FL stores substantially less elastic energy than the human ITB during walking, it resembles the human ITB in being relatively thick and fibrous compared with other deep fascia in the lower limb. Both the chimp FL and human ITB receive muscle fibers from GMaxCr and TFL, and both insert anteriorly on the tibia. Assuming this anatomy was also present in the last common ancestor of chimps and humans, it is reasonable to hypothesize that the human ITB was elaborated from a chimp-like FL by increasing the sizes of the GMaxCr and TFL muscles inserting in the ITB and by increasing ITB thickness, thereby augmenting the potential of the ITB for energy storage.

In addition to differences in muscle morphology, differences in bipedal gait patterns influence the energy storage potential of the human ITB and chimp FL. Chimps, like other primates, walk with a crouched posture and limited hip flexion/extension excursion (Schmitt, 1999; Sockol et al., 2007), reducing stretch and energy storage in the chimp FL compared with the human ITB. Since the last common ancestor of humans and apes almost certainly used a crouched gait, the FL of this species was likely to be stretched a similar amount during walking. FL energy storage would have increased in hominins with more upright postures and larger GMax muscles. However, because the FL does not fossilize and no skeletal markers of this trait have been identified, it is not possible to identify when the ITB evolved in hominin evolution beyond inferences drawn from extant taxa.

A number of skeletal features in australopiths and *Homo* suggest an increased capacity for FL energy storage relative to a chimp-like last common ancestor. Features indicating an extended lower limb posture in hominins include a posteriorly oriented ischium (Robinson, 1972), a large femoral bicondylar angle (valgus knee) (Heiple and Lovejoy, 1971; Stern and Susman, 1983), anteroposteriorly flattened femoral condyles (Heiple and Lovejoy, 1971; Ward, 2002), a more perpendicular orientation of the tibia's distal articular surface relative to the long axis of the tibial shaft (Latimer et al., 1987) and longitudinally oriented trabecular struts in

The Journal of Experimental Biology (2015) 218, 2382-2393 doi:10.1242/jeb.117952

the distal tibia (Barak et al., 2013). Expanded muscle attachment areas on the ilium for GMax and TFL suggest an increase in the force-generating capacity of these muscles.

When did these features first appear in the fossil record? The oldest known hominin species for which we have pelvic material, *Ardipithecus ramidus*, probably had inferiorly oriented ischia like chimpanzees (Lovejoy et al., 2009), but in *Australopithecus afarensis*, the posteriorly oriented ischia (Robinson, 1972; Stern and Susman, 1983), the large bicondylar angle (Stern and Susman, 1983) and the perpendicular orientation of the tibia's distal articular surface relative to the tibial shaft (Latimer et al., 1987) suggest a more upright posture than chimpanzees. The distally flattened femoral condyles (Heiple and Lovejoy, 1971) and longitudinally oriented trabecular struts in the distal tibia (Barak et al., 2013) in *Australopithecus africanus* provide additional evidence that hominins by 2- to 3-million years ago had a human-like extended limb posture. Thus, fossil evidence suggests that australopiths walked with a human-like gait in terms of hip, knee and ankle angles (Latimer et al., 1987; Tardieu and Trinkaus, 1994; Crompton et al., 1998; Ward, 2002; Carey and Crompton, 2005; Barak et al., 2013), likely resulting in increased FL energy storage during walking compared with a chimp-like last common ancestor. However, without increases in the mass of muscles inserting in the FL, which fossil evidence indicates occurred later in the genus *Homo*, FL energy storage would not have reached human-like magnitudes. Pelvises from *Homo erectus* indicate that the GMaxCr attachment surface is broadened and human like (Day, 1973; Rose, 1984; Lieberman et al., 2006), suggesting increased GMaxCr mass and force transmission to the FL.

In summary, our synthesis of experimental data from cadaveric specimens and energy calculations from musculoskeletal models has revealed a novel function for the uniquely human ITB and has identified biomechanical features that increase the potential for energy storage in the human ITB relative to the chimp FL. Although the upright posture of australopiths would have increased FL energy storage during bipedal walking to some extent, only in *Homo* is there evidence of an increase in the size of muscles transmitting force through the FL. The forces transmitted by the human ITB during walking and especially during running, are substantial: we have previously estimated that the ITB stores about 14% as much energy as the Achilles tendon during fast running (up to 7 J; Eng et al., 2015), which suggests that the ITB may be specialized to increase the endurance running capabilities in *Homo*. In future studies, comparative analyses of a broader range of musculoskeletal models, based on data derived from chimpanzees and other higher primate species, offer much potential to advance our understanding of locomotor shifts in the fossil record.

MATERIALS AND METHODS

Moment arm measurements

Detailed measurements of muscle moment arms and anatomy were collected from four fresh-frozen chimpanzee [*Pan troglodytes* (Blumenbach 1775)] cadaveric pelvises (Table 2) obtained from the Texas Biomedical Research Institute (San Antonio, TX). Moment arms of the portions of TFL, GMaxCr and GMAXCd inserting on the FL were determined for hip flexion/extension, hip rotation, hip adduction/abduction and knee flexion/extension using the tendon excursion method (Brand et al., 1975; An et al., 1984).

In each specimen, skin and subcutaneous fat were dissected from the gluteal region and thigh to expose the muscle origins and insertions. The surface of the FL was cleaned of subcutaneous fat, and its insertion on the tibia was exposed distally. Each muscle was separated into portions based on origins and insertions (Table 3). Muscle portions were each represented by a Kevlar thread path for tendon excursion measurements. We anchored Kevlar thread to a screw eye located at the insertion of the MTU, routed the thread through plastic tubing to a screw eye located at the origin of the MTU, and attached it to one of two cable-extension position transducers (PTX101, Celesco, Canoga Park, CA) that measured length changes with an accuracy of ±0.32 mm while applying a tension of 1.4 or 2.8 N. The tubing ensured a repeatable path and decreased friction between the thread and underlying tissues. The 3D coordinates of each muscle path were digitized relative to segment coordinate systems, using a motion-tracking system (Polhemus Fastrak, Colchester, VT) and were used to accurately recreate the paths in the musculoskeletal model. We placed marker pairs in the anterior and posterior FL and tracked their locations with high-speed video (Photron USA Inc., San Diego, CA) while moving the limb through its ranges of hip and knee motion. These data were used to determine the hip and knee angles at which the anterior and posterior FL began to stretch.

Each specimen was mounted in a custom frame as described in Eng et al. (2015), which allowed independent control of hip rotation, hip flexion/extension, hip abduction/adduction and knee flexion/extension after proper specimen alignment (Fig. 10). Briefly, the pelvis was mounted on a table using threaded fixation half-pins (IMEX Veterinary, Inc., Longview, TX). The femur was fixed to the inner of two concentric rings mounted on a rotating cart. Rotating the inner ring relative to the outer ring rotated the femur. Rotating the cart flexed and extended the hip when the specimen was mounted for hip flexion and abducted and adducted the hip when the specimen was mounted for hip adduction. Vertical translation of the rings on the cart adducted or flexed the hip when mounted for hip flexion or adduction, respectively.

Electromagnetic receivers were rigidly attached to the pelvis, femur and tibia, and were used to track the segment's positions and orientations in space using a motion-tracking system. Joint angles were computed from receiver data using custom LabView software (National Instruments, Austin, TX). Anatomical landmarks on each segment were marked with screws and digitized to define each segment's coordinate system based on anatomical axes. To find the hip joint center, the coordinates of the knee joint center (the midpoint between the medial and lateral epicondyles) were recorded while moving the femur through a range of hip flex/extension and hip abuction/adduction angles. A sphere was fitted to this cloud of knee joint center points, and the center of this sphere was defined as the hip joint center and the origin of the femoral coordinate system.

Specimen alignment was performed with real-time feedback of the segment positions and orientations as described in Eng et al. (2015). After aligning the specimen, we monitored coupling of hip angles and ensured that hip adduction varied <2 deg and hip rotation <4 deg over a 75 deg range of flexion. When the specimen was aligned for hip abduction/adduction, we ensured that hip flexion varied <2 deg and hip rotation <4 deg over a 50 deg range of abduction/adduction.

Excursion and joint angle data were simultaneously sampled at 10 Hz using an A/D converter (National Instruments BNC-2090). While moment arms were measured about one joint axis, the other joints were secured at the approximate joint positions found in midstance during bipedal walking (hip flexion, 35 deg; hip rotation, 0 deg; hip adduction, −15 deg; knee flexion, 45 deg) (O'Neill et al., 2015). Lengthening excursion versus joint angle

Table 2. Demographic information for the four chimpanzee cadaveric limbs used in this study

Specimen number	Sex	Age (years)	Height (cm)*	Mass (kg)	Cause of death
1	F	27	137.6	60.0	Heart problems
2	M	23	142.2	81.0	Heart problems
3	F	42	128.2	52.0	Heart problems
4	F	45	124.4	48.0	Heart and kidney problems

*Height was measured as the distance from the top of the head to the bottom of the calcaneus with the limbs extended.

The Journal of Experimental Biology (2015) 218, 2382-2393 doi:10.1242/jeb.117952

Table 3. Origins and insertions of the chimp FL MTU paths used in moment arm measurements

MTU	Origin	Insertion
TFL1	Anterior ilium 1.5 cm medial to ASIS	Proximal lateral tibia, 3 cm posterior to tibial tuberosity
TFL2	Anterior ilium 3.5 cm medial and 3 cm inferior to ASIS	Proximal lateral tibia, 3 cm posterior to tibial tuberosity
GMaxCr1	Posterior ilium, 1 cm medial and 1.5 cm inferior to PSIS	Distal femur 2 cm anterior to lateral epicondyle
GMaxCd3	Proximal ischial tuberosity	Distal femur 1 cm anterior to lateral epicondyle
GMaxCd4	Distal ischial tuberosity	Distal femur 1 cm anterior to lateral epicondyle

data were fitted with a fourth-order polynomial and the derivative of the polynomial was averaged across trials to estimate the moment arm. A minimum of five trials was collected for each condition from each muscle.

Comparative muscle anatomy and muscle architecture

We measured muscle architecture of the chimp TFL, GMaxCr and GMaxCd to estimate each muscle's force-generating capacity. After measuring moment arms, each muscle was carefully dissected to its insertion on the femur or fascia lata (FL). Blunt dissection was used to identify and separate the muscle fibers inserting on the FL from those inserting in the femur. Insertion on the FL was confirmed by placing traction on the separated fibers and ensuring that force was transmitted distally through the FL and not to the tendon inserting in the femur. The portions of TFL and GMax inserting on the FL and femur were weighed, and these masses were summed to calculate the total mass of each muscle. Muscle masses were normalized by body mass and these data were compared with the relative masses of the TFL and GMax inserting on the human ITB reported in Eng et al. (2015).

After measuring muscle length (L_M), a single fascicle was dissected from each muscle portion and measured to obtain fascicle length (L_f) for the region. Because the muscle tissue was unfixed, sarcomere lengths could not be accurately measured to normalize fascicle lengths. The PCSA of each muscle region was calculated using the following equation (Powell et al., 1984):

$$\text{PCSA} = \frac{M}{\rho \cdot L_f}. \quad (1)$$

where M is the region's muscle mass, L_f is the region's average fascicle length and ρ is muscle density (1.056 g cm^{-3}; Mendez and Keys, 1960). Surface pennation angle was measured with a goniometer as the angle between the fascicles and the distal FL. Pennation angle was not included in the PCSA calculation used to estimate the muscle's peak isometric force in the model, since our modeling software SIMM (Software for Interactive Musculoskeletal Modeling v7.0, MusculoGraphics, Santa Rosa, CA) multiplies PCSA, specific tension and pennation angle to determine a muscle's maximum isometric force. However, pennation angle was included in the PCSA calculation used to compare force-generating capacity between humans and chimps. PCSA was scaled to (body mass)$^{2/3}$ assuming geometric similarity in order to compare the relative force-generating capacity of muscle regions between chimps and humans. Normalized muscle PCSAs were compared between chimps and humans using a one-tailed unpaired t-test. All data are presented as means±s.e.m., with $P<0.05$ considered significant.

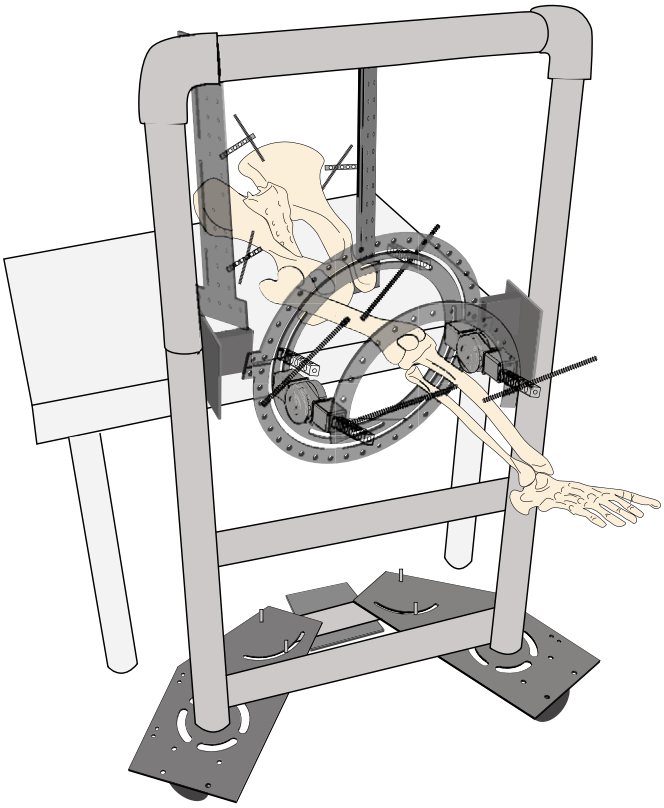

Fig. 10. Chimpanzee lower limbs were mounted in a frame for measuring muscle moment arms. The custom-made frame comprises a fixed platform for aligning and securing the pelvis, an adjustable cart for moving the femur through a range of hip flex/extension and abduction/adduction angles, and a set of concentric rings for rotating the femur about its mechanical axis, following Arnold et al. (2000).

Representation of MTU paths in the musculoskeletal model

We modified paths of the TFL–FL and GMax–FL MTUs in the musculoskeletal model reported by O'Neill et al. (2013) to match our digitized muscle attachments, regional paths and moment arm data (Fig. 11). Using SIMM, we created two paths for TFL, one path for GMaxCr, and two paths for GMaxCd. MTUs were represented as line segments spanning from origin to insertion and were constrained by 'via' points (points through which a muscle is constrained to act) and wrap objects to simulate underlying structures and more accurately estimate changes in length with changes in joint angle (supplementary material Fig. S1). Via points and wrapping surfaces were iteratively adjusted so that the paths resembled the paths digitized during the experiments and the model's moment arms

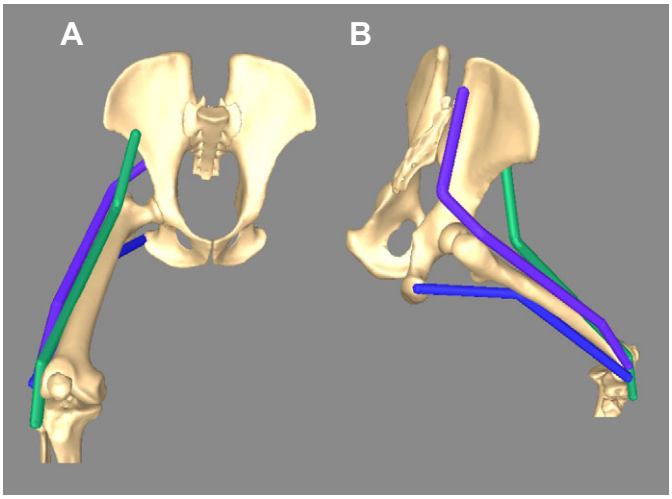

Fig. 11. The chimp lower extremity model modified from O'Neill et al. (2013). (A) Anterolateral view of the chimp lower extremity model showing TFL–FL$_{ant}$ (green), GMaxCr–FL$_{ant}$ (purple) and GMaxCd–FL$_{post}$ (blue). (B) Posterolateral view of the chimp model showing the FL MTU paths.

matched the moment arms determined experimentally. The experimentally measured moment arms were used to adjust the model's paths and verify their accuracy. Our refined model is available on SimTK (simtk.org).

Although multiple muscle paths were created and analyzed to gain insight into FL–MTU 3D anatomy, paths were combined to represent the three major paths of chimp FL force transmission that we observed in our experiments, including the two anterior FL paths (GMaxCr–FL_{ant} and TFL1 and TFL2 combined as TFL–FL_{ant}) and the posterior FL path (GMaxCd3,4; GMaxCd–FL_{post}). We iteratively made small adjustments to the via points and wrapping objects of the anterior and posterior FL paths to yield combined MTU paths with average moment arms.

We used a Hill-type muscle model (Zajac, 1989; Delp et al., 1990) to estimate isometric forces generated by TFL–FL_{ant}, GMaxCr–FL_{ant} and GMaxCd–FL_{post}. Active and passive force–length curves were scaled to each FL MTU path using two key parameters, maximum isometric force (F_{max}) and optimal fiber length (L_{opt}). We used measured fascicle lengths for L_{opt}, and we calculated F_{max} as the product of each muscle region *PCSA* and the muscle-specific tension of 31.5 N cm^{-2} used in O'Neill et al. (2013). F_{max} and tendon slack length (L_{TS}) were used to scale each MTU's 'tendon' force–length curve. Tendon slack lengths were chosen for each MTU such that the FL began to stretch passively at hip and knee angles consistent with our experimental measurements. We verified that these L_{TS} values allow the muscles in our model to generate force over functional ranges of motion.

For each MTU, we created a normalized force–length curve for the chimp FL as described in Eng et al. (2015). We used an elastic modulus (E) of 400 MPa, which is consistent with values of 369–398 MPa reported in the literature for the human ITB (Butler et al., 1984; Derwin et al., 2008; Hammer et al., 2012; Steinke et al., 2012). Above a transition strain of 3%, we assumed a linear relationship between force and strain with a normalized stiffness ($\tilde{k}$) determined using the elastic modulus (E), the muscle F_{max}, and the effective cross-sectional area of the FL (a):

$$\tilde{k} = \frac{E \cdot a}{F_{max}}.$$

For each MTU, the effective cross-sectional area of the FL was calculated from measurements of regional thickness and width in cadaveric specimens (supplementary material Table S1). Thickness was measured with a micrometer and the width of each FL region was measured while placing tension on the inserting muscle and visually assessing FL strain with video.

The capacity of the FL to store elastic energy during bipedal walking

We used our model along with joint kinematics and EMG activations to estimate the ability of the FL to store and recover elastic energy during bipedal walking. First, we calculated the origin-to-insertion lengths of the MTUs at hip and knee angles typical of chimps during bipedal walking (O'Neill et al., 2015). We identified periods of the stride when MTUs were near maximum length and also likely active (Stern and Susman, 1981) and we assumed that peak strains in FL_{ant} or FL_{post} would occur at these times. Next, we separated the MTU lengths into FL lengths and muscle fiber lengths by independently activating each MTU in the model and solving for the lengths at which the muscle force and FL force were equivalent, accounting for pennation angle. We set each muscle's activation to 20%, 40% and 60% (of its maximum activation) to assess FL strains during walking. We estimated energy storage capacity at each activation level by integrating the FL and ITB force–length curves from L_{TS} to the peak FL or ITB length during walking. Peak energy storage in the anterior and posterior chimp FL was normalized by the chimp model's body mass of 55 kg and compared with similar estimates of mass-specific peak energy storage in the anterior and posterior human ITB (normalized by the human model's body mass of 83 kg) derived from the data reported in Eng et al. (2015).

The capacity of the human ITB and the chimp FL to generate a frontal plane moment at the hip

To assess whether the human ITB is specialized to stabilize the pelvis in the frontal plane compared with the chimp FL, we examined the moment-generating capacity of the FL and ITB MTUs about an anterior–posterior axis through the hip joint center when the muscles are fully activated at the joint positions found in midstance. These frontal plane moments were compared with the total frontal plane moment generated by all of the other hip abductors when fully activated. Moments were normalized by body weight and hemi-pelvis width (the distance between the hip joint center and midline of the pelvis).

Acknowledgements

The authors dedicate this manuscript to Farish A. Jenkins Jr (1940–2012) who provided many stimulating and insightful discussions during C.M.E.'s dissertation research, which provided the basis for this study. The authors thank two anonymous reviewers for constructive comments that significantly improved this manuscript. The authors also gratefully acknowledge Delande Justinvil and Zachary Lewis for technical assistance during the moment arm experiments. We are grateful for the assistance of Casey Boyle and Yasmin Rawlins during pilot studies, and we thank Dr Andrew Mountcastle and Glenna Clifton for help with videography. We thank Dr Thomas Roberts for his helpful comments on this manuscript.

Competing interests

The authors declare no competing or financial interests.

Author contributions

C.M.E., A.S.A., A.A.B., and D.E.L. designed the study. C.M.E. and A.S.A. conducted the experiments. C.M.E. modified the musculoskeletal model. C.M.E. and A.S.A. analyzed the data. C.M.E. wrote the manuscript. A.S.A., A.A.B. and D.E.L. revised the manuscript.

Funding

This work was supported by a Wenner–Gren Dissertation Fieldwork Grant [8588 to C.M.E.].

Supplementary material

Supplementary material available online at
http://jeb.biologists.org/lookup/suppl/doi:10.1242/jeb.117952/-/DC1

References

Almécija, S., Tallman, M., Alba, D. M., Pina, M., Moyà-Solà, S. and Jungers, W. L. (2013). The femur of Orrorin tugenensis exhibits morphometric affinities with both Miocene apes and later hominins. *Nat. Commun.* **4**, 2888.

An, K. N., Takahashi, K., Harrigan, T. P. and Chao, E. Y. (1984). Determination of muscle orientations and moment arms. *J. Biomech. Eng.* **106**, 280-282.

Arnold, A. S., Salinas, S., Hakawa, D. J. and Delp, S. L. (2000). Accuracy of muscle moment arms estimated from MRI-based musculoskeletal models of the lower extremity. *Comput. Aided Surg.* **5**, 108-119.

Arnold, E. M., Ward, S. R., Lieber, R. L. and Delp, S. L. (2010). A model of the lower limb for analysis of human movement. *Ann. Biomed. Eng.* **38**, 269-279.

Barak, M. M., Lieberman, D. E., Raichlen, D. A., Pontzer, H., Warrener, A. G. and Hublin, J.-J. (2013). Trabecular evidence for a human-like gait in *Australopithecus africanus*. *PLoS ONE* **8**, e77687.

Berge, C. and Penin, X. (2004). Ontogenetic allometry, heterochrony, and interspecific differences in the skull of African apes, using tridimensional Procrustes analysis. *Am. J. Phys. Anthropol.* **124**, 124-138.

Biewener, A. A. and Roberts, T. J. (2000). Muscle and tendon contributions to force, work, and elastic energy savings: a comparative perspective. *Exerc. Sport Sci. Rev.* **28**, 99-107.

Bodine, S. C., Roy, R. R., Eldred, E. and Edgerton, V. R. (1987). Maximal force as a function of anatomical features of motor units in the cat tibialis anterior. *J. Neurophysiol.* **6**, 1730-1745.

Brand, P. W., Cranor, K. C. and Ellis, J. C. (1975). Tendon and pulleys at the metacarpophalangeal joint of a finger. *J. Bone Joint Surg. Am.* **57**, 779-784.

Butler, D. L., Grood, E. S., Noyes, F. R., Zernicke, R. F. and Brackett, K. (1984). Effects of structure and strain measurement technique on the material properties of young human tendons and fascia. *J. Biomech.* **17**, 579-596.

Carey, T. S. and Crompton, R. H. (2005). The metabolic costs of 'bent-hip, bent-knee' walking in humans. *J. Hum. Evol.* **48**, 25-44.

Champneys, F. (1871). The muscles and nerves of a Chimpanzee (*Troglodytes Niger*) and a *Cynocephalus Anubis*. *J. Anat. Physiol.* **6**, 176-211.

Crompton, R. H., Yu, L., Weijie, W., Günther, M. M. and Savage, R. (1998). The mechanical effectiveness of erect and "bent-hip, bent-knee" bipedal walking in *Australopithecus afarensis*. *J. Hum. Evol.* **35**, 55-74.

Darwin, C. (1871). *The Descent of Man and Selection in Relation to Sex*. London: Murray.

Day, M. H. (1973). Locomotor features of the lower limb in hominids. *Symp. Zool. Soc. Lond* **33**, 29-51.

Delp, S. L., Loan, J. P., Hoy, M. G., Zajac, F. E., Topp, E. L. and Rosen, J. M. (1990). An interactive graphics-based model of the lower extremity to study orthopaedic surgical procedures. *IEEE Trans. Biomed. Eng.* **37**, 757-767.
Derwin, K. A., Baker, A. R., Spragg, R. K., Leigh, D. R., Farhat, W. and Iannotti, J. P. (2008). Regional variability, processing methods, and biophysical properties of human fascia lata extracellular matrix. *J. Biomed. Mater. Res. A.* **84A**, 500-507.
Eng, C. M., Arnold, A. S., Lieberman, D. E. and Biewener, A. A. (2015). The capacity of the human iliotibial band to store elastic energy during running. *J. Biomech.* doi:10.1016/j.jbiomech.2015.06.017.
Farris, D. J. and Sawicki, G. S. (2012). Human medial gastrocnemius force–velocity behavior shifts with locomotion speed and gait. *Proc. Natl. Acad. Sci. USA* **109**, 977-982.
Gottschalk, F., Kourosh, S. and Leveau, B. (1989). The functional anatomy of tensor fasciae latae and gluteus medius and minimus. *J. Anat.* **166**, 179-189.
Greaser, M. L., Moss, R. L. and Reiser, P. J. (1988). Variations in contractile properties of rabbit single muscle fibres in relation to troponin T isoforms and myosin light chains. *J. Physiol.* **406**, 85-98.
Haile-Selassie, Y. (2001). Late Miocene hominids from the Middle Awash, Ethiopia. *Nature* **412**, 178-181.
Hammer, N., Lingslebe, U., Aust, G., Milani, T. L., Hädrich, C. and Steinke, H. (2012). Ultimate stress and age-dependent deformation characteristics of the iliotibial tract. *J. Mech. Behav. Biomed. Mater.* **16**, 81-86.
Heiple, K. G. and Lovejoy, C. O. (1971). The distal femoral anatomy of Australopithecus. *Am. J. Phys. Anthropol.* **35**, 75-84.
Holowka, N. B. and O'Neill, M. C. (2013). Three-dimensional moment arms and architecture of chimpanzee (*Pan troglodytes*) leg musculature. *J. Anat.* **223**, 610-628.
Hoy, M. G., Zajac, F. E. and Gordon, M. E. (1990). A musculoskeletal model of the human lower extremity: the effect of muscle, tendon, and moment arm on the moment-angle relationship of musculotendon actuators at the hip, knee, and ankle. *J. Biomech.* **23**, 157-169.
Inman, V. T. (1947). Functional aspects of the abductor muscles of the hip. *J. Bone Joint Surg. Am.* **29**, 607-619.
Kaplan, E. B. (1958). The iliotibial tract: clinical and morphological significance. *J. Bone Joint Surg. Am.* **40**, 817-832.
Latimer, B., Ohman, J. C. and Lovejoy, C. O. (1987). Talocrural joint in African hominoids: implications for Australopithecus afarensis. *Am. J. Phys. Anthropol.* **74**, 155-175.
Lichtwark, G. A., Bougoulias, K. and Wilson, A. M. (2007). Muscle fascicle and series elastic element length changes along the length of the human gastrocnemius during walking and running. *J. Biomech.* **40**, 157-164.
Lieberman, D. E., Raichlen, D. A., Pontzer, H., Bramble, D. M. and Cutright-Smith, E. (2006). The human gluteus maximus and its role in running. *J. Exp. Biol.* **209**, 2143-2155.
Lovejoy, C. O. (2009). Reexamining human origins in light of Ardipithecus ramidus. *Science* **326**, 74, 74e1-74e8.
Lovejoy, C. O., Suwa, G., Simpson, S. W., Matternes, J. H. and White, T. D. (2009). The great divides: *Ardipithecus ramidus* reveals the postcrania of our last common ancestors with African apes. *Science* **326**, 73, 100-106.
Lucas, S. M., Ruff, R. L. and Binder, M. D. (1987). Specific tension measurements in single soleus and medial gastrocnemius muscle fibers of the cat. *Exp. Neurol.* **95**, 142-154.
Mendez, J. and Keys, A. (1960). Density and composition of mammalian muscle. *Metabolism.* **9**, 184-188.
O'Neill, M. C., Lee, L.-F., Larson, S. G., Demes, B., Stern, J. T. and Umberger, B. R. (2013). A three-dimensional musculoskeletal model of the chimpanzee (*Pan troglodytes*) pelvis and hind limb. *J. Exp. Biol.* **216**, 3709-3723.
O'Neill, M. C., Lee, L.-F., Demes, B., Thompson, N. E., Larson, S. G., Stern, J. T., Jr and Umberger, B. R. (2015). Three-dimensional kinematics of the pelvis and hind limbs in chimpanzee (*Pan troglodytes*) and human bipedal walking. *J Hum. Evol.* (in press).
Payne, R. C., Crompton, R. H., Isler, K., Savage, R., Vereecke, E. E., Günther, M. M., Thorpe, S. K. S. and D'Août, K. (2006). Morphological analysis of the hindlimb in apes and humans. II. Moment arms. *J. Anat.* **208**, 725-742.
Pilbeam, D. (1996). Genetic and morphological records of the Hominoidea and hominid origins: a synthesis. *Mol. Phylogenet. Evol.* **5**, 155-168.
Pontzer, H. (2007). Predicting the energy cost of terrestrial locomotion: a test of the LiMb model in humans and quadrupeds. *J. Exp. Biol.* **210**, 484-494.
Pontzer, H., Raichlen, D. A. and Rodman, P. S. (2014). Bipedal and quadrupedal locomotion in chimpanzees. *J. Hum. Evol.* **66**, 64-82.
Powell, P. L., Roy, R. R., Kanim, P., Bello, M. and Edgerton, V. R. (1984). Predictability of skeletal muscle tension from architectural determinations in guinea pig hindlimbs. *J. Appl. Physiol.* **57**, 1715-1721.
Preuschoft, H. (1961). Muskeln und Gelenke der Hinterextremitat des Gorillas. *Morphol. Jahrbuch* **101**, 432-540.
Robinson, J. T. (1972). *Early Hominid Posture and Locomotion*. Chicago: University of Chicago Press.
Rodman, P. S. and McHenry, H. M. (1980). Bioenergetics and the origin of hominid bipedalism. *Am. J. Phys. Anthropol.* **52**, 103-106.
Rolian, C., Lieberman, D. E., Hamill, J., Scott, J. W. and Werbel, W. (2009). Walking, running and the evolution of short toes in humans. *J. Exp. Biol.* **212**, 713-721.
Rose, M. D. (1984). A hominine hip bone, KNM-ER 3228, from East Lake Turkana, Kenya. *Am. J. Phys. Anthropol.* **63**, 371-378.
Ruvolo, M. (1994). Molecular evolutionary processes and conflicting gene trees: the hominoid case. *Am. J. Phys. Anthropol.* **94**, 89-113.
Satta, Y., Klein, J. and Takahata, N. (2000). DNA archives and our nearest relative: the trichotomy problem revisited. *Mol. Phylogenet. Evol.* **14**, 259-275.
Sayers, K. and Lovejoy, C. O. (2008). The chimpanzee has no clothes: a critical examination of *Pan troglodytes* in models of human evolution. *Curr. Anthropol.* **49**, 87-114.
Schmitt, D. (1999). Compliant walking in primates. *J. Zool.* **248**, 149-160.
Shea, B. T. (1985). Ontogenetic allometry and scaling. In *Size and Scaling in Primate Biology* (ed. W. L. Jungers), pp. 175-205. Springer.
Sigmon, B. A. (1974). A functional analysis of pongid hip and thigh musculature. *J. Hum. Evol.* **3**, 161-185.
Sigmon, B. A. (1975). Functions and evolution of hominid hip and thigh musculature. In *Primate Functional Morphology and Evolution* (ed. R. H. Tuttle), pp. 235-252. Paris: Mouton.
Sigmon, B. A. and Farslow, D. L. (1986). *The Primate Hindlimb*. New York: A.R. Liss.
Sockol, M. D., Raichlen, D. A. and Pontzer, H. (2007). Chimpanzee locomotor energetics and the origin of human bipedalism. *Proc. Natl. Acad. Sci. USA* **104**, 12265-12269.
Spoor, C. W., van Leeuwen, J. L., Meskers, C. G. M., Titulaer, A. F. and Huson, A. (1990). Estimation of instantaneous moment arms of lower-leg muscles. *J. Biomech.* **23**, 1247-1259.
Steinke, H., Lingslebe, U., Böhme, J., Slowik, V., Shim, V., Hädrich, C. and Hammer, N. (2012). Deformation behavior of the iliotibial tract under different states of fixation. *Med. Eng. Phys.* **34**, 1221-1227.
Stern, J. T., Jr. (1972). Anatomical and functional specializations of the human gluteus maximus. *Am. J. Phys. Anthropol.* **36**, 315-339.
Stern, J. T., Jr and Susman, R. L. (1981). Electromyography of the gluteal muscles in Hylobates, Pongo, and Pan: implications for the evolution of hominid bipedality. *Am. J. Phys. Anthropol.* **55**, 153-166.
Stern, J. T., Jr and Susman, R. L. (1983). The locomotor anatomy of *Australopithecus afarensis*. *Am. J. Phys. Anthropol.* **60**, 279-317.
Swindler, D. R. and Wood, C. D. (1973). *An Atlas of Primate Gross Anatomy: Baboon, Chimpanzee, and Man*. Seattle: University of Washington Press.
Tardieu, C. and Trinkaus, E. (1994). Early ontogeny of the human femoral bicondylar angle. *Am. J. Phys. Anthropol.* **95**, 183-195.
Taylor, C. R. and Rowntree, V. J. (1973). Running on two or on four legs: which consumes more energy? *Science* **179**, 186-187.
Taylor, C. R., Heglund, N. C. and Maloiy, G. M. O. (1982). Energetics and mechanics of terrestrial locomotion. I. Metabolic comsumption as a function of speed and size in birds and mammals. *J. Exp. Biol.* **97**, 1-21.
Thorpe, S. K. S., Crompton, R. H., Günther, M. M., Ker, R. F. and Alexander, R. M. (1999). Dimensions and moment arms of the hind- and forelimb muscles of common chimpanzees (*Pan troglodytes*). *Am. J. Phys. Anthropol.* **110**, 179-199.
Ward, C. V. (2002). Interpreting the posture and locomotion of *Australopithecus afarensis*: where do we stand? *Yearb. Phys. Anthropol.* **119**, 185-215.
Wrangham, R. W. and Pilbeam, D. (2001). African apes as time machines. In *All Great Apes Great and Small, Volume I: African Apes* (ed. B. Galdikas, N. Briggs, L. Sheeran, G. Shapiro and J. Goodall), pp. 5-17. New York: Kluwer Academics/ Plenum Publishers.
Zajac, F. E. (1989). Muscle and tendon: properties, models, scaling, and application to biomechanics and motor control. *Crit. Rev. Biomed. Eng.* **17**, 359-411.
Zollikofer, C. P. E., Ponce de León, M. S., Lieberman, D. E., Guy, F., Pilbeam, D., Likius, A., Mackaye, H. T., Vignaud, P. and Brunet, M. (2005). Virtual cranial reconstruction of *Sahelanthropus tchadensis*. *Nature* **434**, 755-759.